Characterization of Asian dust and Siberian smoke with multi-wavelength Raman lidar over Tokyo, Japan in spring 2003

Toshiyuki Murayama,[1] Detlef Müller,[2] Katsuya Wada,[1] Atsushi Shimizu,[3] Miho Sekiguchi,[1] and Tatsuro Tsukamoto[1]

[1] In the spring of 2003, we observed lofted Asian dust and Siberian forest-fire smoke plumes in the free troposphere over Tokyo, Japan with a dual-wavelength Raman lidar. These data show clear signatures of the optical characteristics depending on the aerosol type. The Asian-dust layer shows that the particle depolarization ratio (PDR) at 532 nm is ~20%, and the extinction-to-backscatter ratio (lidar ratio) at 355 nm is ~49 sr, which is close to ~43 sr measured at 532 nm. On the contrary, the smoke layers show that the PDR is as small as 5–8% or less, and the lidar ratio at 355 nm is ~40 sr, which is considerably lower than ~65 sr which was measured at 532 nm. We also applied an inversion algorithm for the smoke case. The effective radius was ~0.22 μm and the single-scattering albedo at 532 nm was ~0.95. *INDEX TERMS:* 0305 Atmospheric Composition and Structure: Aerosols and particles (0345, 4801); 0368 Atmospheric Composition and Structure: Troposphere—constituent transport and chemistry; 0394 Atmospheric Composition and Structure: Instruments and techniques. **Citation:** Murayama, T., D. Müller, K. Wada, A. Shimizu, M. Sekiguchi, and T. Tsukamoto (2004), Characterization of Asian dust and Siberian smoke with multi-wavelength Raman lidar over Tokyo, Japan in spring 2003, *Geophys. Res. Lett.*, *31*, L23103, doi:10.1029/2004GL021105.

1. Introduction

[2] Aerosols play an important role in the Earth's radiation budget because they scatter and absorb light, and present a key uncertainty in the assessment of radiative forcing [*Intergovernmental Panel on Climate Change (IPCC)*, 2001]. They also serve as cloud condensation nuclei and modulate the cloud properties. East Asia is considered as a region where emission of anthropogenic aerosols is rapidly increasing due to growing economy. Recently, the Asia-Pacific Regional Aerosol Characterization Experiment (ACE-Asia) showed that the spatial variability of aerosol composition and properties is rather high in this area [*Huebert et al.*, 2003; *Murayama et al.*, 2003]. It has also been shown that mineral dust has an indirect effect on clouds by serving as effective ice nuclei [*Sassen et al.*, 2002, 2003; *Murayama et al.*, 2001; *Sakai et al.*, 2004]. Therefore, it is highly important to study not only column-averaged but also height-resolved aerosol optical properties regularly.

[3] Nowadays, sophisticated multi-wavelength Raman lidars enable us to characterize tropospheric aerosols by the observable quantities themselves, and in further to retrieve microphysical properties from them [*Müller et al.*, 2001; *Mattis et al.*, 2002, 2003]. From the point of view of feasibility, we installed a UV-Raman lidar system that emits the third harmonic frequency (355 nm) on the basis of a second Nd:YAG laser in addition to our existing lidar system at Tokyo University of Marine Science and Technology (TUMST; 35.66°N, 139.80°E) [*Murayama et al.*, 1999]. Thus our lidar system is capable of measuring backscatter coefficients at 355, 532, 1064 nm, extinction coefficients at 355 and 532 nm, particle depolarization ratio at 532 nm, and water–vapor mixing ratio, simultaneously. To our knowledge, this is the first dual-wavelength Raman lidar installed in East Asia. In this short contribution, we demonstrate how the dual-wavelength Raman lidar can be used for the characterization of optical properties of aerosols observed during regional aerosol events that occurred successively. We briefly outline the lidar system in section 2. Section 3 presents results of observations for Asian dust and Siberian forest-fire smoke in the spring of 2003 with emphasis on the aerosol characterization by observed aerosol optical properties, and the microphysical parameters of the smoke derived from the inversion code.

2. Measurements and Data Processing

[4] We installed the UV-Raman lidar system next to the existing Mie-Polarization-Raman lidar, which uses the laser beams at 532 (VIS) and 1064 nm (IR) wavelength [*Murayama et al.*, 1999; *Wada and Murayama*, 2004]. The repetition frequencies of the laser pulses are 10 Hz. The data were stored every 4,094 shots, i.e., ~7 minutes. Both analog and photon-counting methods of the photo-multipliers are employed with transient recorders (TR20-160, Licel). Typical operating laser powers are approximately 100, 100, 200 mJ per pulse for the 355, 532 and 1064 nm laser beams. Full overlap between the telescope field of view and the laser beams occurs 1–1.5 km height depending on the receivers. The backscatter ratio at 355 nm and the water-vapor mixing ratio are evaluated down to ~100 m above ground level, because we can take the geometrical form factor identical for the channels that detect the elastic signal and the inelastic Raman signals. However, it is not the case for the 532-nm backscatter ratio, because we used different receivers for the elastic and the N_2-Raman channels [*Murayama et al.*, 1999].

[5] The extinction coefficient and the backscatter ratio of the aerosols at 355 and 532 nm, and the mixing ratio are derived with the methods described by *Ansmann et al.* [1992] and *Whiteman et al.* [1992, 2003]. The atmospheric

---
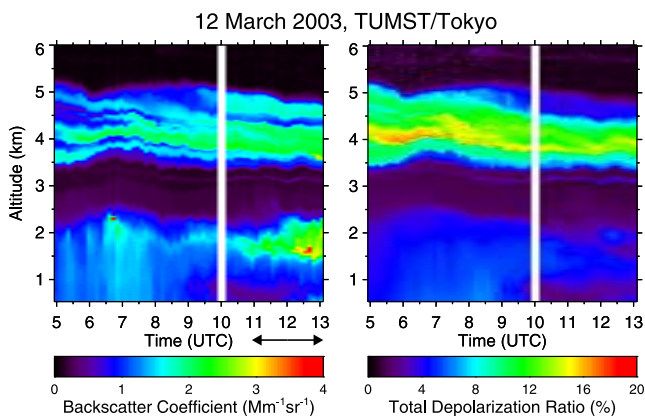
Figure 1. Time-height cross section of aerosol backscatter coefficients and total depolarization ratios at 532 nm over TUMST in Tokyo, Japan on 12 March 2003. Vertical resolution and temporal resolution is 30 m and ~7 minutes, respectively. The horizontal arrow indicates the time period integrated for the Raman lidar evaluations.

density profile was calculated from routine radiosonde observations at Tateno (36.05°N, 140.12°E; ~60 km away from TUMST) at 12 UTC. The extinction profiles at 355 and 532 nm were derived for the Asian dust case after applying a sliding average to the range-corrected N_2-Raman signals for 5 points (600 m) above 5.0 and 1.4 km, respectively. Similarly, for the smoke case, the extinction profiles at 355 and 532 nm were derived after applying the sliding average to the range-corrected N_2-Raman signals for 3 points (360 m) only above 4.5 and 3.7 km, respectively. The backscatter coefficient at 1064 nm is obtained from the Mie-Rayleigh signal by using the method proposed by *Fernald* [1984] and assuming a lidar ratio of 40 sr.

[6] The lidar-derived water-vapor mixing ratio is normalized so that the lowest value (~75 m above the lidar) matches to the surface observation with a well-calibrated hygrometer at TUMST and by assuming an error of ±10%. Then the relative humidity was calculated using the temperature and pressure profiles obtained from the radiosonde data. Deviations of the mixing ratio and relative humidity

obtained from the lidar at TUMST to the respective quantities derived with radiosonde at Tateno (see figures later in the text) can be attributed to the spatial distance of the two sites and different measurement times, and the unknown error of the calibration factor of the lidar.

3. Results and Discussion

3.1. Case of Asian Dust

[7] Figure 1 presents the time-height cross section of the backscatter coefficient and the total (particle + molecular) depolarization ratio at 532 nm, respectively, on 12 March 2003. The depolarization ratio is an indicator of irregularly shaped particles. Figure 2 shows the mean profiles of aerosol optical properties for a measurement period from 1056 to 1306 UTC. We also calculated the Ångström exponent (AE) and the backscatter-related Ångström exponent (BAE) from the profiles of the extinction and backscatter coefficients at 355 and 532 nm, respectively. The error bars are based on statistical and estimated systematic errors. The aerosol layer between 3 and 5 km seems to be composed of two layers as indicated by the horizontal dashed lines A and B in Figure 2: layer A is rather narrow with the peak at 4.6 km, layer B is broader with the peak at 4.0 km. The lower layer B carries features of mineral dust as suggested from the high particle depolarization ratio (PDR > 20%), while the PDR in layer A is as small as 6%. The mean lidar ratios at 355 (S_{355}) and 532 nm (S_{532}) were nearly the same within the standard deviations, i.e., 48.6(±8.5) and 43.1(±7.0) sr, respectively, in the dust-like layer (3.5–4.3 km). The value of PDR and S_{532} is similar to our previous observations [*Murayama*, 2002; *Murayama et al.*, 2003]. The value of S_{355} is close to the lidar ratio observed for Saharan dust at 351 nm in southern Italy (~50 sr) [*De Tomasi et al.*, 2003], but smaller than what was observed in Leipzig, Germany (50–80 sr) [*Mattis et al.*, 2002]. *Mattis et al.* [2002] also found that S_{355} is 10–30% higher than S_{532}. The difference in the lidar ratio values might be attributed to differences in shape, size or absorption properties of mineral particles.

[8] In addition, Figure 2 shows another interesting differences of the aerosol optical properties besides the large
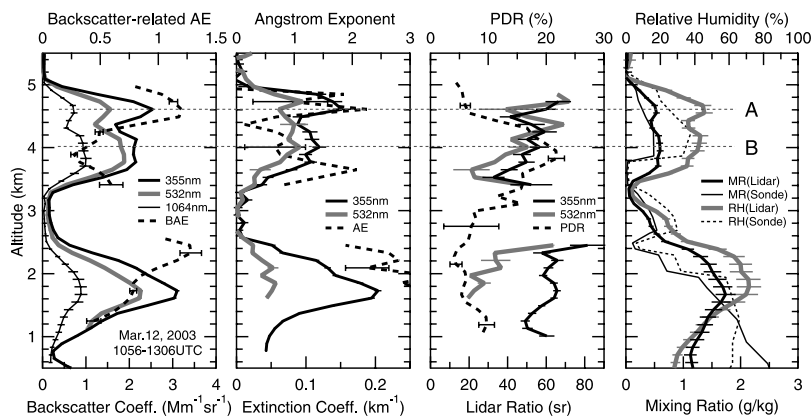
Figure 2. Mean profiles of the aerosol optical properties (backscatter coefficients, extinction coefficients, backscatter-related Ångström exponent (355–532 nm), Ångström exponent, lidar ratios, particle depolarization ratio), water-vapor mixing ratio and relative humidity for the measurement from 1056 to 1306 UTC on 12 March 2003. The height resolution of the profiles is 120 m. The mixing ratio and relative humidity obtained from radiosonde at Tateno (12 UTC) are shown for reference.
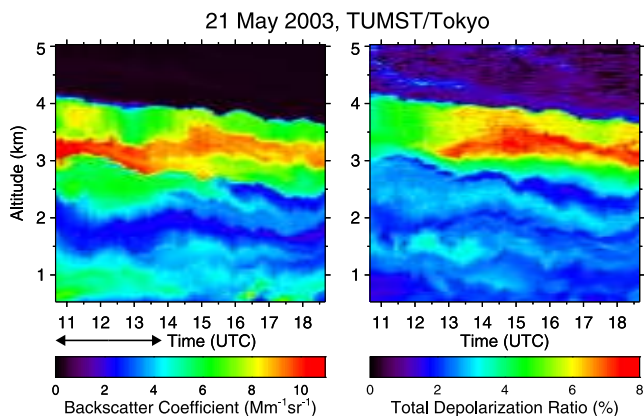
Figure 3. As in Figure 1, except for 21 May 2003.

difference of the PDR in the layers A and B. The BAE in layer A (~1.2) is higher than in layer B (~0.3), which suggests that layer A might be composed of smaller aerosols. Since the relative humidity in layers A and B are nearly identical (~40%), we can reject the assumption that hygroscopic growth of mineral dust reduces the depolarization ratio.

3.2. Case of Forest-Fire Smoke

[9] In the spring and summer of 2003, an unusually high number of forest fires occurred in Siberia [*Mattis et al.*, 2003]. Smoke plumes originating from these fires were transported over Japan with westerly wind. Figure 3 shows a time-height plot of the backscatter coefficient and the total depolarization ratio at 532 nm on 21 May 2003. Back trajectory analyses show that the airmass from 2 to 4 km originated in regions of intense forestfire which occurred from west of Lake Baykal to east of the border of China, Russia and Mongolia (not shown). The smoke layer sharply dropped off at ~4 km. The upper part (3–4 km) of the smoke layer showed a depolarization ratio of about 6%. A similar feature was also observed in Suwon (37.14°N, 127.04°E), Korea [*Lee et al.*, 2004].

[10] Figure 4 shows the mean profiles of the optical properties for a measurement from 1040 to 1349 UTC. There is a prominent layer between 2.5 and 4 km. The intensive parameters, i.e., S_{532}, PDR, AE show optical

properties, which change at the height of ~3.2 km where extensive parameters, i.e., particle backscatter and extinction coefficients reach their maximum values. The upper part of the particle layer, except for the rim, had the following features: i) BAE is high (~1.9) while AE is small (~0.7), ii) S_{532} (~65 sr) is higher than S_{355} (~40 sr), iii) PDR is ~6%. On the other hand, in the lower part, S_{532} and PDR drop to ~40 sr and ~3%, respectively, while AE increases to ~1.2.

[11] The relationship between S_{355} and S_{532}, i.e., $S_{532} > S_{355}$, and the non-negligible particle depolarization ratio is consistent with lidar observations of aged smoke from Canada over central Europe during the Lindenberg Aerosol Characterization Experiment LACE98 [*Wandinger et al.*, 2002; *Fiebig et al.*, 2002]. A part of this Siberian smoke was also detected over central Europe and showed the same relationship between S_{355} and S_{532} [*Mattis et al.*, 2003]. The non-zero depolarization ratio might be caused by soil material that was uplifted into the forest fire plume [*Fiebig et al.*, 2002], or the nonsphericity of the particles due to coagulation of smoke particles [*Martins et al.*, 1998]. The latter explanation seems more reasonable because no signature of mineral dust was found from a chemical analysis of aerosols sampled at the summit of Mt. Fuji (3,776 m above sea level and ~100 km west of Tokyo) in the same period (N. Kaneyasu, private communication, 2004).

[12] A small AE (~0.7) as presented here in the wavelength range from 355–532 nm was also found from Sun/ sky photometer observations for cases of heavy smoke in South America and South Africa [*Eck et al.*, 1999]. These authors also reported a significant positive curvature for the relationship of the log(τ_a) versus log(λ). The analysis of the collocated TUMST skyradiometer (POM-01, Prede) daytime observations with respect to this relationship shows a similar tendency (not shown).

[13] We applied the method of inversion with regularization only for the case of smoke to retrieve the microphysical properties using the backscatter coefficients at 355, 532, 1064 nm and the extinction coefficients at 355 and 532 nm [*Müller et al.*, 2001; *Wandinger et al.*, 2002; *Veselovskii et al.*, 2002]. For the moment we cannot apply the inversion code for the case of Asian dust which possesses a high PDR, i.e., the particle have a non-spherical shape, because it
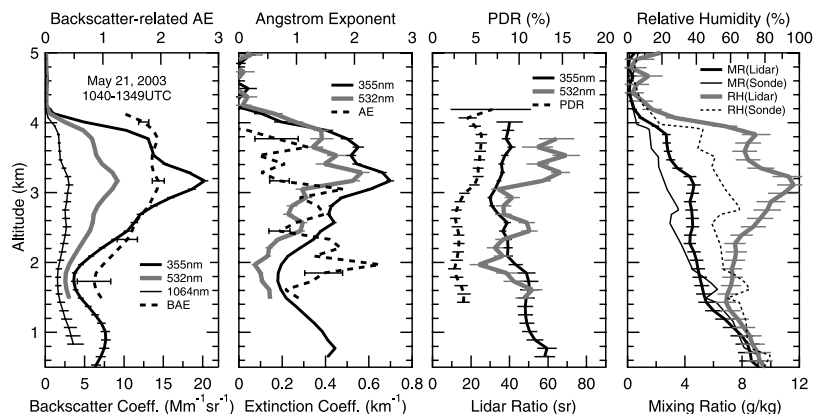
Figure 4. As in Figure 2, except for the period from 1040 to 1349 UTC on 21 May 2003.
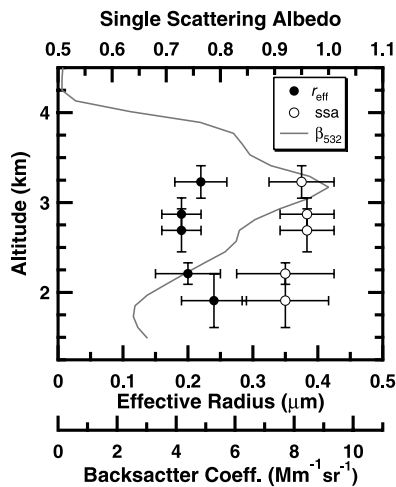
Figure 5. Vertical variation of microphysical particle properties for the lidar measurements from 1040 to 1349 UTC on 21 May 2003 over TUMST in Tokyo, Japan. Horizontal error bars are the standard deviation of the parameters. Vertical error bars describe the height ranges across which the optical data were averaged and used for the data inversion.

has been developed for the case of particles of spherical shape. We found 0.22(±0.04) μm for the effective radius (surface-weighted mean radius) and 0.95(±0.06) for the single scattering albedo (SSA) at 532 nm around the peak of the smoke layer. Figure 5 shows effective radius and single scattering albedo for selected height ranges. The results indicate that particles in the accumulation mode are dominant, which is a typical feature for the case of smoke. The relatively high SSA indicates low absorbing particles.

[14] For comparison, the typical mean radius and the SSA of Asian dust plumes obtained by intensive airborne in situ measurements during ACE-Asia were 2−3 μm and 0.96(±0.01) at 550 nm, respectively [*Murayama et al.*, 2003; *Anderson et al.*, 2003].

4. Summary

[15] The distinct optical signatures for mineral dust and aged smoke presented here demonstrate how multi-wavelength Raman lidar can be used for a height-resolved characterization of tropospheric aerosols. For the Asian dust case we found a high PDR of more than 20% at 532 nm and a small wavelength dependence of the lidar ratio between 355 and 532 nm (43−49 sr), for the smoke case we found a small PDR less than 5−8% and a high wavelength dependence of the lidar ratio: S_{355} is ~40 sr, while S_{532} is ~65 sr. We also successfully derived the climate-relevant microphysical parameters, e.g. effective radius and single scattering albedo, for the smoke case. Mean values of the effective radius varied between 0.2−0.25 μm and the mean single scattering albedo was 0.92−0.97 at 532 nm. Such advanced Raman lidar is an essential tool for the character-ization of the complex aerosols found over East Asia and have great potential for application in global aerosol lidar networking in future.

References

Anderson, T. L., et al. (2003), Variability of aerosol optical properties derived from in situ aircraft measurements during ACE-Asia, *J. Geophys. Res.*, *108*(D23), 8647, doi:10.1029/2002JD003247.

Ansmann, A., et al. (1992), Combined Raman elastic-backscatter lidar for vertical profiling of moisture, aerosol extinction, backscatter, and lidar ratio, *Appl. Phys.*, *B55*, 18−28.

De Tomasi, F., A. Blanco, and M. R. Perrone (2003), Raman lidar monitor-ing of extinction and backscattering of African dust layers and dust characterization, *Appl. Opt.*, *42*, 1699−1709.

Eck, T. F., et al. (1999), Wavelength dependence of the optical depth of biomass burning, urban, and desert dust aerosols, *J. Geophys. Res.*, *104*(D24), 31,333−31,349.

Fernald, F. G. (1984), Analysis of atmospheric lidar observations: Some comments, *Appl. Opt.*, *23*, 652−653.

Fiebig, M., et al. (2002), Optical closure for an aerosol column: Method, accuracy, and inferable properties applied to a biomass-burning aerosol and its radiative forcing, *J. Geophys. Res.*, *107*(D21), 8130, doi:10.1029/2000JD000192.

Huebert, B. J., et al. (2003), An overview of ACE-Asia: Strategies for quantifying the relationship between Asian aerosols and their climate impacts, *J. Geophys. Res.*, *108*(D23), 8633, doi:10.1029/2003JD003550.

Intergovernmental Panel on Climate Change (IPCC) (2001), *Climate Change 2001: The Scientific Basis*, 896 pp., Cambridge Univ. Press, New York.

Lee, C. H., et al. (2004), Continuous measurements of smoke of Russian forest fire by 532/1064 nm Mie scattering lidar at Suwon, Korea, in *Reviewed and Revised Papers Presented at the 22nd International Laser Radar Conference, ESA SP-561*, edited by G. Pappalardo and A. Amodeo, pp. 535−538, Eur. Space Agency, Paris.

Martins, J. V., et al. (1998), Sphericity and morphology of smoke particles from biomass burning in Brazil, *J. Geophys. Res.*, *103*(D24), 32,051−32,057.

Mattis, I., et al. (2002), Dual-wavelength Raman lidar observations of the extinction-to-backscatter ratio of Saharan dust, *Geophys. Res. Lett.*, *29*(9), 1306, doi:10.1029/2002GL014721.

Mattis, I., et al. (2003), Unexpectedly high aerosol load in the free tropo-sphere over central Europe in spring/summer 2003, *Geophys. Res. Lett.*, *30*(22), 2178, doi:10.1029/2003GL018442.

Müller, D., et al. (2001), Comprehensive particle characterization from three-wavelength Raman-lidar observations: Case study, *Appl. Opt.*, *40*, 4863−4869.

Murayama, T. (2002), Optical properties of Asian dust aerosol lofted over Tokyo observed by Raman lidar, in *Lidar Remote Sensing in Atmospheric and Earth Sciences: Proceedings of the 21th ILRC*, edited by L. R. Bissonnette, G. Roy, and G. Vallée, pp. 331−334, Defense R&D Canada, Valcartier, Québec, Canada.

Murayama, T., et al. (1999), Application of lidar depolarization measure-ment in the atmospheric boundary layer: Effects of dust and sea-salt particles, *J. Geophys. Res.*, *104*(D24), 31,781−31,792.

Murayama, T., et al. (2001), Ground-based network observation of Asian dust events of April 1998 in east Asia, *J. Geophys. Res.*, *106*(D16), 18,345−18,359.

Murayama, T., et al. (2003), An intercomparison of lidar-derived aerosol optical properties with airborne measurements near Tokyo during ACE-Asia, *J. Geophys. Res.*, *108*(D23), 8651, doi:10.1029/2002JD003259.

Sakai, T., et al. (2004), Raman lidar measurement of water vapor and ice clouds associated with Asian dust layer over Tsukuba, Japan, *Geophys. Res. Lett.*, *31*, L06128, doi:10.1029/2003GL019332.

Sassen, K. (2002), Indirect climate forcing over the western US from Asian dust storms, *Geophys. Res. Lett.*, *29*(10), 1465, doi:10.1029/2001GL014051.

Sassen, K., et al. (2003), Saharan dust storms and indirect aerosol effects on clouds: CRYSTAL-FACE results, *Geophys. Res. Lett.*, *30*(12), 1633, doi:10.1029/2003GL017371.

Veselovskii, I., et al. (2002), Inversion with regularization for the retrieval of tropospheric aerosol parameters from multiwavelength lidar sounding, *Appl. Opt.*, *41*, 3685−3699.

Wada, K., and T. Murayama (2004), Optical properties of tropospheric aerosols observed with UV-Raman lidar in Tokyo, in *Reviewed and Revised Papers Presented at the 22nd International Laser Radar Conference, ESA SP-561*, edited by G. Pappalardo and A. Amodeo, pp. 427–430, Eur. Space Agency, Paris.

Wandinger, U., et al. (2002), Optical and microphysical characterization of biomass-burning and industrial-pollution aerosols from multiwavelength lidar and aircraft measurements, *J. Geophys. Res.*, *107*(D21), 8125, doi:10.1029/2000JD000202.

Whiteman, D. N. (2003), Examination of the traditional Raman lidar technique. I. Evaluating the temperature-dependent lidar equations, *Appl. Opt.*, *42*, 2571–2593.

Whiteman, D. N., S. H. Melfi, and R. A. Ferrare (1992), Raman lidar system for the measurement of water vapor and aerosols in the Earth's atmosphere, *Appl. Opt.*, *31*, 3068–3082.

———————————

D. Müller, Institute for Tropospheric Research, Permoserstr. 15, 04318 Leipzig, Germany.

T. Murayama, M. Sekiguchi, T. Tsukamoto, and K. Wada, Faculty of Marine Technology, Tokyo University of Marine Science and Technology, 2-1-6 Etchujima, Koto, Tokyo 135-8533, Japan.

A. Shimizu, National Institute for Environmental Studies, 16-2 Onogawa, Tsukuba, Ibaraki 305-8506, Japan.